Comparison of ultrasound attenuation tomography methods for breast imaging

Cuiping Li[a], Neb Duric[b], and Lianjie Huang[c]
[a]Karmanos Cancer Institute, 4100 John R. Street, 4 HWCRC, Detroit, MI 48201; Phone: 313-576-8768, Emails: lic@karmanos.org
[b]Karmanos Cancer Institute, 4100 John R. Street, 4 HWCRC, Detroit, MI 48201; Phone: 313-576-8706, Emails: duric@karmanos.org
[c]Mail Stop D443, Los Alamos National Laboratory, Los Alamos, NM87545; Phone: 505-665-1108; Email: ljh@lanl.gov

ABSTRACT

Ultrasound attenuation parameters of breast masses are closely related to their types and pathological states, therefore, it is essential to reliably estimate attenuation parameters for quantitative breast tissue characterization. We study the applicability of three different attenuation tomography methods for ultrasound breast imaging using a ring transducer array. The first method uses the amplitude decays of signals transmitted through the breast to reconstruct attenuation coefficients. The second method employs the spectral ratios between the pulse propagating through the breast and that through water to obtain attenuation parameters. The third method makes use of the complex energy ratios estimated using the amplitude envelopes of transmitted signals. We use *in vitro* and *in vivo* breast data acquired with a clinical ultrasound breast imaging system (CURE) to compare these tomography methods. Our results show that the amplitude decay method yields attenuation coefficients with more artifacts than the other two methods. There is bias and variability in the estimated attenuation using the spectral ratio due to its sensitivity to different temporal band-widths and signal-to-noise-ratios of the data. The method based on the complex signal energy ratio is more robust than the other two methods and yields images with fewer artifacts.

Keywords*:* Amplitude decay, breast cancer, complex signal energy ratio, spectral ratio, ultrasound attenuation.

1. INTRODUCTION

Discrimination of benign and malignant breast masses is very difficult using conventional ultrasound images. Attenuation imaging using transmission ultrasound signals is an alternative imaging modality that helps in differentiating cancer from benign tumors. Attenuation measurements have been studied by a number of groups[1-9] using various techniques.

In this study, we compare the performance of three ultrasound attenuation tomography approaches that are respectively based on the (a) amplitude decay, (b) spectral ratio, and (c) complex signal energy ratio. Amplitude decay is the most straightforward attenuation tomography method. In our implementation of the spectral ratio method, we improve its performance by dynamically selecting the length of the time window and bandwidth used for the spectral ratio analysis. In the third method, we calculate the total signal energy using the amplitude envelope of the corresponding analytic signal. The amplitude envelop is used because of its natural separation from signal phase and frequency information, and its insensitivity to small phase shifts. Since the average amplitude envelope is phase and frequency independent, it is more stable in terms of susceptibility to noise contamination when compared to the real signal (real part of the analytic signal). This idea is derived from the B-mode ultrasound imaging that utilizes RF envelope as the "reflection strength."

We conduct attenuation reconstructions using these three tomography techniques. *In vitro and in vivo* ultrasound breast data used are acquired with a clinical prototype ring array called Computerized Ultrasound Risk Evaluation (CURE). In this ring array, an ultrasound pulse emits sequentially from the transducer elements to the breast from various directions

Medical Imaging 2008: Ultrasonic Imaging and Signal Processing, edited by Stephen A. McAleavey, Jan D'hooge, Proc. of SPIE Vol. 6920, 692015, (2008) · 1605-7422/08/$18 · doi: 10.1117/12.771433

and the transmitted signals are recorded. For the first two tomography methods, we assume that the ultrasound attenuation in the breast increases linearly with the frequency:

$$a(f) = a_0 \mid f \mid, \tag{1}$$

where parameter a_0 is the attenuation coefficient. The linear dependence in soft tissues (like the breast) in the low MHz range has been experimentally verified and reported by many investigators[1, 10-12]. In our study, we also assume the transmission coefficients at all water-tissue and tissue-tissue interfaces are one.

2. ATTENUATION ESTIMATION

2.1 CURE ring array

A detailed description of the CURE ultrasound breast imaging system can be found in Duric et. al.[13]. A brief overview is outlined here to clarify the transducer geometry. The CURE device was developed and built at the Karmanos Cancer Institute (KCI). This clinical prototype is a near real-time device that has been integrated into the patient flow of KCI'sWalt Comprehensive Breast Center. Figure 1 is a picture of the CURE ring transducer. The 20-cm-diameter ring consists of 256 equally-spaced and water-coupled transducer elements, and is immersed in a water tank. During the scan, the patient is positioned prone with the breast situated through a hole in the canvas bedding. This results in the breast being suspended in water, inside the imaging tank, and also encircled by the ring. A motorized gantry translates the ring in the vertical direction, starting from the chest wall through the breast's nipple region. During scanning at each step, the 256 transducer elements sequentially emit fan beam ultrasound signals with a central frequency of 1.5 MHz toward the opposite side of the ring. The forward scattered (transmission) and backscattered (reflection) ultrasound signals are subsequently recorded by all 256 elements at a sampling rate of 6.25 MHz.

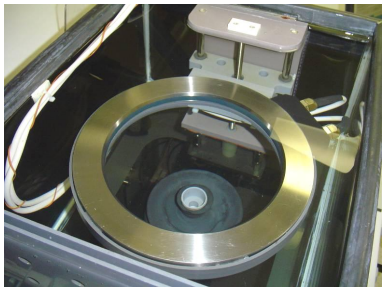

Figure 1. A picture of CURE transducer ring array.

We assume that there is no attenuation in the water shots, and attenuation parameters estimation is carried out relative to the water shots. Water shot data is obtained by collecting ultrasound data right before the breast scan. The advantage using water shots as the base for attenuation is that the first-order geometrical spreading has been removed. In all three attenuation methods, we ignore high-order geometrical spreading terms.

2.2 Localization of the first-arrival pulse by the amplitude envelope method

Both attenuation tomography methods based on the spectral ratio and the complex signal energy ratio require localization of the first-arrival pulse for each transmission waveform.

A real waveform $y(t)$ can be represented by its amplitude envelope $a(t)$ and phase $\theta(t)$:

$$y(t) = a(t)\cos\theta(t). \tag{2}$$

The corresponding quadrature waveform can be expressed as

$$y^*(t) = a(t)\sin\theta(t) = -H(y(t)), \tag{3}$$

where $H(y(t))$ is the Hilbert transform of $y(t)$. The corresponding analytic waveform $z(t)$ is then give by

$$z(t) = y(t) + iy^*(t). \tag{4}$$

The amplitude envelope can be derived as[14]

$$a(t) = \sqrt{y(t)^2 + y^*(t)^2}. \tag{5}$$

To isolate the first-arrival pulse, the beginning of the pulse is obtained by the pulse's first arrival pick. The end of the pulse is determined by taking the time difference between the start of the pulse and the first envelope peak, then multiplying by a factor[15]. Figure 2 is an example of isolating a first-arrival pulse. . The dashed curve in Fig. 2 is the amplitude envelope, and the two vertical solid lines indicate the selected time window (isolated first-arrival pulse).

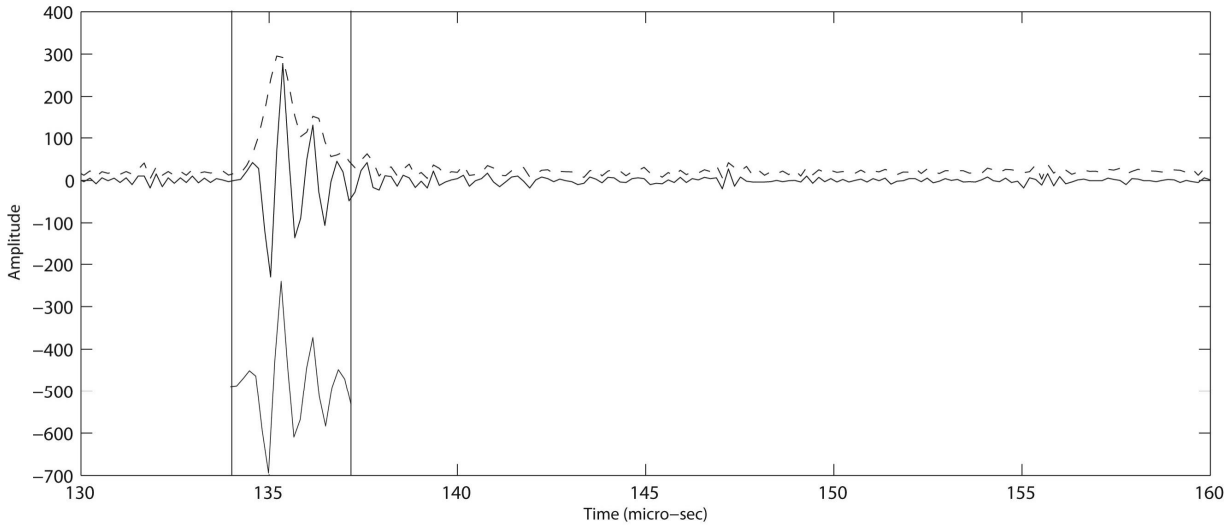

Figure 2. An example of amplitude envelope. Solid curve is the real waveform, and dashed curve is the corresponding amplitude envelope. Segment between the two vertical lines is the isolated first-arrival pulse.

2.3 Amplitude decay method

Ultrasound attenuation can be expressed as

$$A_r = A_s e^{-f_c \int_{ray} a_0 dl}, \tag{6}$$

where A_r is the received waveform amplitude, A_s is the source amplitude measured in a water shot at the same receiver, f_c is the central frequency, a_0 is attenuation parameter to be reconstructed, and l is the length of the ultrasound ray path.

In the amplitude decay method, data are assumed to be sufficiently band-limited, so energy concentrates at a central frequency f_c. After rearranging and taking the natural logarithm on both sides of eq. (6), the attenuation parameter a_0 can be estimated as

$$\int_{ray} a_0 dl = \frac{1}{f_c} \ln \frac{A_s}{A_r}. \tag{7}$$

2.4 Spectral ratio method

For the case of a linear frequency dependency (eq. (1)), eq. (7) becomes

$$f\int_{ray} a_0 dl = \ln\frac{A_s(f)}{A_r(f)}, \tag{8}$$

or

$$Y(f) = Cf, \tag{9}$$

where $Y(f) = \ln\frac{A_s(f)}{A_r(f)}$ is the natural logarithm of the source (water shot in our case) and received amplitude spectra ratio, and $C = \int_{ray} a_0 dl$ is the integrated attenuation along the ray path. By fitting a least-squares line through $Y(f)$ versus f, C can be obtained from the slope of the line.

The time window used to obtain $A_s(f)$ and $A_r(f)$ can affect the calculated attenuation values estimated from the spectral ratios. First, by using a short time window, the secondary arrivals can be removed. This in turn removes spectral holes that result from interfering pulses that can cause problems when performing a line fit to the spectral ratio. However, too short a time window can cause the spectral ratios to become highly variable[16], and also cause a poor sampling at lower frequencies. We dynamically locate the first-arrival pulse for each waveform using the method described in section 2.2.

Another variable greatly influencing the attenuation estimation is the spectral bandwidth used to perform the linear regression. We make use of the largest bandwidth of the data to improve the reliability of estimated attenuation values. Since the spectrum of the waveform varies with the angular position of the receiver, a fixed spectral bandwidth may cause instability in the attenuation estimation. With a fixed bandwidth, some of the usable spectrum may not be included for some waveforms, while the bandwidth may be too large for others. We dynamically determine the largest usable bandwidth for each individual waveform based on its noise level. The lower and upper cut-off frequencies of the bandwidth are selected at the points where the amplitude spectrum is reduced to the noise level.

2.5 Complex signal energy ratio method

As discussed in section 2.2, analytic waveforms can be obtained by eq. (4). In the method proposed in this section, the signal energy of the analytic waveform for the first-arrival pulse is calculated. The complex energy ratio between the breast data and the corresponding water shot is used to estimate the attenuation coefficient.

The total complex energy for the water shot is

$$E_W = \int_{t_2}^{t_1} |I(t)|^2 \, dt, \tag{10}$$

where t_1 and t_2 define the time window that isolates the first arrival, and I is the corresponding amplitude envelope. Similarly, the total complex energy for breast data is

$$E_B = \int_{t_1'}^{t_2'} |R(t)|^2 \, dt, \tag{11}$$

where t_1', t_2', R are the same parameters as in eq. (10) but for the breast data. The first-arrival pulse is selected using the method discussed in section 2.2.

The integrated attenuation is defined as

$$\int_{ray} a_0 dl = \log_{10}(\frac{E_w}{E_B}) / f_n, \tag{12}$$

where f_n is the Nyquist frequency which is 3.125 MHz for the CURE device.

2.6 Solving the inverse problem using a bent-ray tomography method

After the integrated attenuation $C = \int_{ray} a_0 dl$ is estimated using the above methods, attenuation parameter a_0 can be obtained by solving the discretized inverse problem

$$\sum_j l_{ij} a_{0j} = C_i, \tag{13}$$

where a_{0j} is the attenuation parameter for the j^{th} model cell, and l_{ij} is the ray length of the i^{th} ray within the j^{th} cell.

We use a bent-ray tomography algorithm to reconstruct attenuation parameters. We first use the time of flight of the transmission ultrasound signals to reconstruct the sound-speed distribution, then trace the bent ray path based on the reconstructed sound-speed model and eq. (13) to obtain the attenuation parameter a_0.

3. COMPARISON OF *IN VITRO* AND *IN VIVO* APPLICATIONS

3.1 Phantom study

The attenuation tomography methods based on the amplitude decay, spectral ratio, and complex signal energy ratio are first applied to breast phantom data acquired using the CURE device. The breast phantom was built by Dr. Ernest Madsen of the University of Wisconsin, which provides tissue-equivalent scanning characteristics of highly scattering, predominantly parenchymal breast tissue. A cross-section of X-ray CT scan is shown in Fig. 3a, which includes two low attenuation fat inclusions (1 & 2), and two high attenuation tumors (3 & 4). The high/low attenuations of the inclusions are relative to their surrounding breast tissue.

The attenuation estimations for the breast phantom using three different methods are shown in Figs. 3b-3d, respectively. Visual appearance shows that complex signal energy ratio method (Fig. 3d) provides a better estimation than the amplitude decay (Fig. 3b) and spectra ratio methods (Fig. 3c). Attenuation estimation by the amplitude decay method in Figure 3b is blurred and inclusion 2 is almost invisible. Attenuation estimated by the spectra ratio method (Fig. 3c) contains a lot of random artifacts in the background, and the relative attenuations for inclusion 1 and 3 have the wrong signs.

3.2 Clinical study

Attenuation estimation was performed on 181 patients' breast data acquired using the CURE device. The breast attenuation images reconstructed using the amplitude decay, spectra ratio and complex signal energy ratio methods are depicted in Figs. 4b, 4c, and 4d, respectively. Figure 4a illustrates the sound-speed reconstruction of the same data set. Figure 5 shows another *in vivo* application example.

Our *in vivo* attenuation study shows that the attenuation tomography method based on the complex signal energy ratio yields noticeably better attenuation images than the amplitude decay and spectra ratio methods. Although it is in general consistent with those estimated by the complex signal energy ratio method, the attenuation images obtained using the amplitude decay method are usually blurred. The attenuation values produced by the spectra ratio method (Fig. 4c and Fig. 5c) are highly variable, and the coherent features can barely be identified.

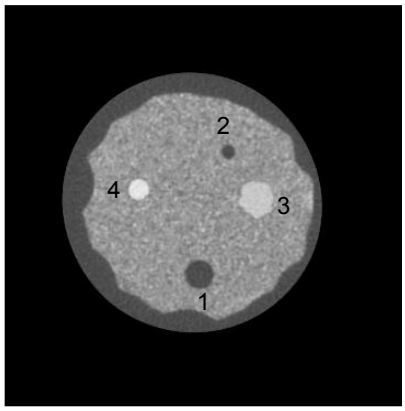

(a) X-ray CT of the breast phantom.

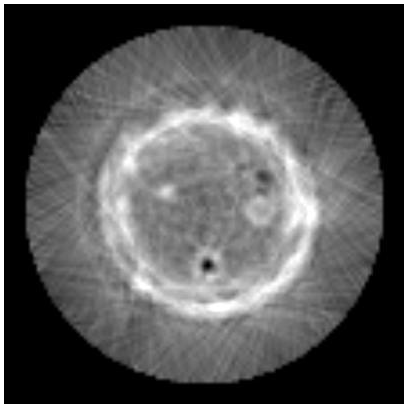

(b) Attenuation estimated by the amplitude decay method.

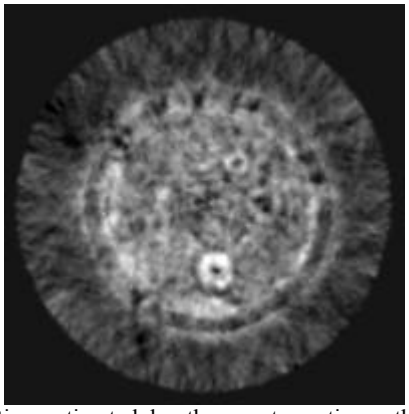

(c) Attenuation estimated by the spectra ratio method.

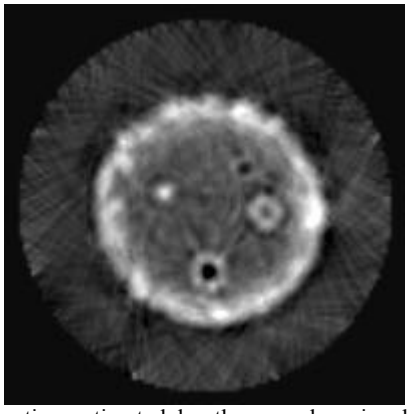

(d) Attenuation estimated by the complex signal energy ratio method.

Figure 3. Comparison of breast-phantom ultrasound attenuation images reconstructed using the amplitude decay, spectral ratio, and complex signal energy ratio methods. In (a), inclusions1 & 2 are low attenuation fat, and 3 & 4 are high attenuation tumors. The attenuation image in (d) is clearly the best. Bright gray-shades stand for high attenuation, and dark areas represent low attenuation.

4. DISCUSSION AND CONCLUSIONS

Our *in vitro* and *in vivo* studies have demonstrated that the attenuation tomography using the amplitude decay is more sensitive to focusing and defocusing effect of the sound-speed structures of the breast. In addition, amplitude decay assumes that the data bandwidths are narrow, which limits its performance because our ultrasound breast data are broadband[1].

The performance of the spectral ratio method depends on many factors. As discussed previously, the temporal window length and the band width for the spectrum analysis are two of the major variables. The spectrum analysis of our ultrasound breast data is very sensitive to the window length, which is mainly due to the lack of calibration of CURE before any data processing. All these factors contribute to the highly scattered attenuation images obtained using the spectral ratio method. To stabilize its performance, variable window lengths and bandwidths need to be used. Device calibration is very important for separating the source signature from the impulse response of the transducer elements. The calibration step is important not only for the spectra ratio method but for all the frequency-domain method such as Kak's energy ratio method[1].

The reason that the attenuation images contain the halo effect around low attenuation regions is because we ignore the out of plane refraction and assume that the in-plane transmission coefficients is one (ignore the reflection). Both assumptions can result in artificially higher attenuation around any interface (halo effect).

Our studies indicate that the attenuation tomography method based on the complex signal energy ratio is the most robust and reliable for reconstructing the ultrasound attenuation distribution of the breast.

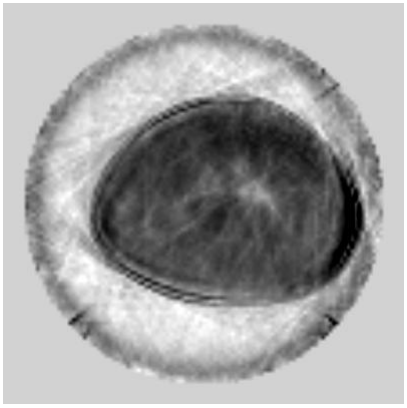

(a) Sound-speed reconstruction.

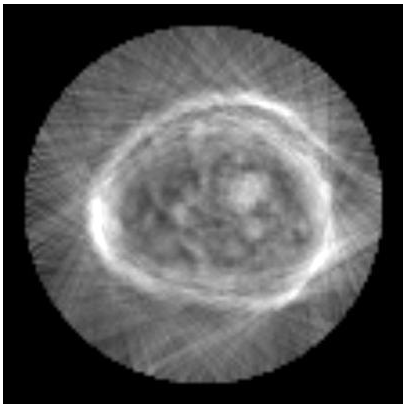

(b) Attenuation estimated by the amplitude decay method.

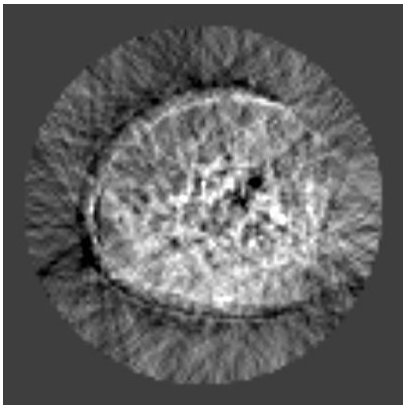

(c) Attenuation estimated by the spectra ratio method.

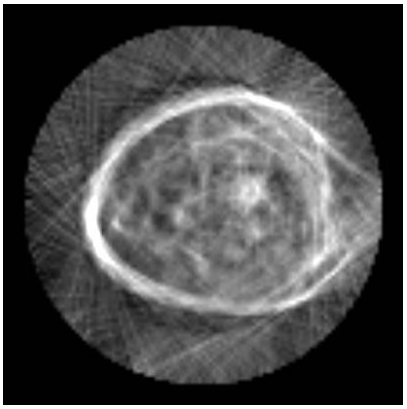

(d) Attenuation estimated by the complex signal energy ratio method.

Figure 4. Comparison of ultrasound attenuation images reconstructed using *in vivo* breast data for Patient A and the amplitude decay, spectra ratio, and complex signal energy ratio methods. Image in (a) is the corresponding sound-speed reconstruction.

ACKNOWLEDGEMENTS

This work was supported through the Karmanos Cancer Institute and a grant from the Michigan Economic Development Corporation (Grant Number 06-1-P1-0653). L. Huang acknowledges the support of U.S. DOE Laboratory-Directed Research and Development program at Los Alamos National Laboratory.

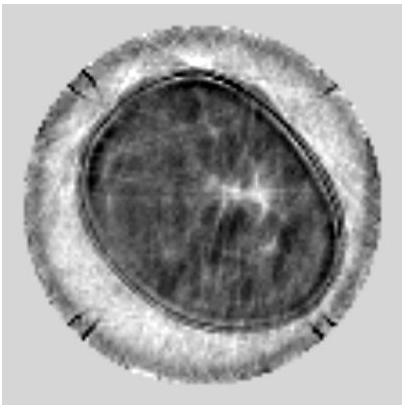

(a) Sound-speed reconstruction.

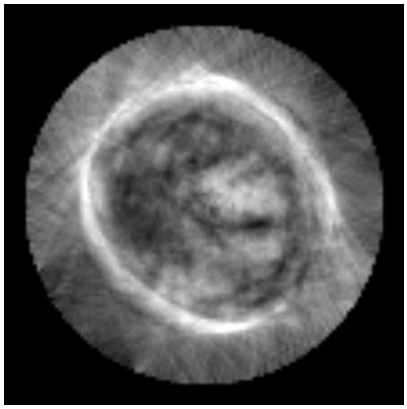

(b) Attenuation estimated by the amplitude decay method.

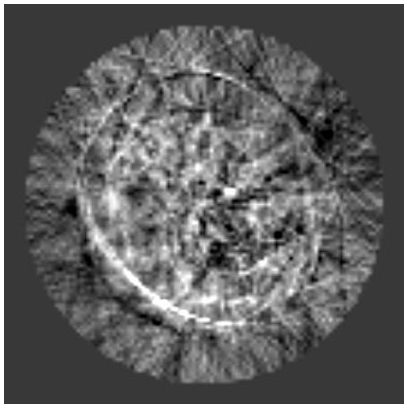

(c) Attenuation estimated by the spectra ratio method.

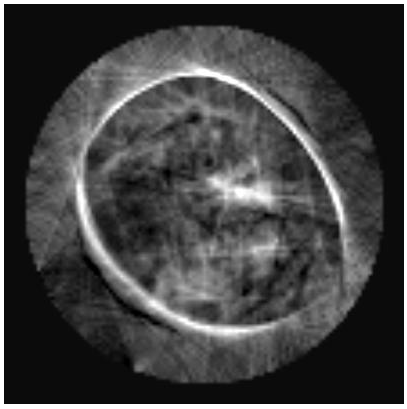

(d) Attenuation estimated by the complex signal energy ratio method.

Figure 5. Comparison of ultrasound attenuation images reconstructed using *in vivo* breast data for Patient B and the amplitude decay, spectra ratio, and complex signal energy ratio methods. Image in (a) is the corresponding sound-speed reconstruction.

REFERENCES

1. Kak, A. C. and Dines, K. A., "Signal Processing of Broadband Pulsed Ultrasound: Measurement of Attenuation of Soft Biological Tissue," IEEE Transaction on Biomedical Engineering 25, 321-344 (1978).
2. Parker, K. J. and Waag, R. C., "Measurement of Ultrasonic Attenuation Within Regions Selected from B-Scan Images," IEEE Transactions on Biomedical Engineering 30, 431-437 (1983).
3. Narayana, P. A., Ophir, J. and Maklad, N. F., "The attenuation of ultrasound in biological fluids," J. Acoust. Soc. Am. 76, 1-4 (1984).
4. Parker, K. J., Lerner, R. M. and Waag, R. C., "Attenuation of Ultrasound Magnitude and Frequency Dependence for Rissue Characterization," Radiology 153, 785-788 (1984).
5. Schreiman, J. S., Gisvold, J. J., Greenleaf, J. F. and Bahn, R. C., "Ultrasound Transmission Computed Tomography of the Breast," Radiology 150, 523-530 (1984).
6. Schmitt, R. M., Meyer, C. R., Carson, P. L. and Chenevert, R. L., "Error Reduction in Through Transmission Tomography Using Large Receiving Arrays with Phase-Insensitive Signal Processing," IEEE Transactions on Sonics and Ultrasonics 31, 251-258 (1984).
7. Parker, K. J., Lerner, R. M. and Waag, R. C., "Comparision of Techniques for In Vivo Attenuation Measurements," IEEE Transactions on Biomedical Engineering 35, 1064-1068 (1988).
8. Walach, E., Shmulewitz, A., Itzchak, Y. and Heyman, Z., "Local Tissue Attenuation Images Based on Pulse-Echo Ultrasound Scans," IEEE Transactions on Biomedical Engineering 36, 211-221 (1989).

9. Fujii, Y., Itoh, K., Shigeta, K., Wang, Y., Tsao, J., Kumasaki, K. and Itoh, R., "A New Method for Attenuation Coefficient Measurement in the Liver," J. Ultrasound Med. 21, 783-788 (2002).
10. Carstensen, E. L., "The Mechanism of the Absorption of Ultrasound in Biological materials," IRE Transactions on Medical Electronics, 158-162 (1960).
11. Dunn, F., "Temperature and Amplitude Dependence of Acoustic Absorption in Tissue," J. Accoust. Soc. Am. 34, 1545-1547 (1962).
12. Goldman, D. E. and Heuter, R. F., "Tabular Data of the Velocity and Absorption of High Frequency Sound in Mammalian Tissue," J. Acoust. Soc. Am. 28, 35-37 (1956).
13. Duric, N., Littrup, P., Poulo, L., Babkin, A., Pevzner, R., Holsapple, E., Rama, O. and Glide, C., "Detection of breast cancer with ultrasound tomography: First results with the Computed Ultrasound Risk Evaluation (CURE) prototype," Medical Physics 34, 773-785 (2007).
14. Taner, M. T., Koehler, F. and Sheriff, R. E., "Complex seismic trace analysis," Geophysics 44, pp.1041-1063, 1979.
15. Matheney M. P. and Nowack, R. L., "Seismic attenuation values obtained from instantaneous-frequency matching and spectral ratios," Geophys. J. Int. 123, 1-15 (1995).
16. Sams, M. and Goldberg, D., "The validity of Q estimates from borehole data using spectral ratios," Geophysics 55, 97-101 (1990).